coatings

MDPI

Article

Robust Superhydrophilic/Underwater Superoleophobic Surface with Anti-Abrasion and Anti-Corrosion Performances Based on Laser Ablation

Duoxun Fang [1], Adham Al-akhali [1], Molin Cao [2], Jiahao Liu [1] and Zhengqiang Tang [1,*]

[1] School of Mechanical Engineering, Guizhou University, Guiyang 550025, China; fangduoxun@163.com (D.F.); adham2055@163.com (A.A.-a.); jiahaoliu1020@163.com (J.L.)
[2] International College of Engineering Technology, Guizhou University, Guiyang 550025, China; linmolinmo031@gmail.com
* Correspondence: zhengqiangtang@126.com

Abstract: Preparing underwater superoleophobic surface is an effective method to solve the problems of oil adhesion on the underwater surfaces and oil spill in water. However, the underwater superoleophobic surfaces at present are not reliable in practical application due to their poor stability under corrosion and abrasion. Herein, we proposed a facile method to fabricate a robust superhydrophilic/underwater superoleophobic surface. The surface is combined with micro honeycomb frame structure and nanostructure, which was fabricated by laser ablation. The surface with the honeycomb pattern shows strong hydrophilicity with a water contact angle of 0° and stable underwater oil repellency with an underwater oil contact angle of 164.9°. Furthermore, it can maintain its excellent underwater superoleophobic performance after 120 cycles of abrasion and corrosion of 6 h at pH = 1–14.

Keywords: superhydrophilic; underwater superoleophobic; laser ablation; anti-fouling

check for updates

Citation: Fang, D.; Al-akhali, A.; Cao, M.; Liu, J.; Tang, Z. Robust Superhydrophilic/Underwater Superoleophobic Surface with Anti-Abrasion and Anti-Corrosion Performances Based on Laser Ablation. *Coatings* **2023**, *13*, 1118. https://doi.org/10.3390/coatings13061118

Academic Editor: Philipp Vladimirovich Kiryukhantsev-Korneev

Received: 9 May 2023
Revised: 9 June 2023
Accepted: 14 June 2023
Published: 17 June 2023

Copyright: © 2023 by the authors. Licensee MDPI, Basel, Switzerland. This article is an open access article distributed under the terms and conditions of the Creative Commons Attribution (CC BY) license (https://creativecommons.org/licenses/by/4.0/).

1. Introduction

Wettability, jointly determined by surface structure and surface chemical components, is an important property for surfaces. Since the first discovery of the lotus effect, manufacturing surfaces with unique wettability became a promising technology in industry application, such as self-clearing [1,2], metal corrosion protection [3–5], surface anti-freezing [6–8], and medical engineering [9–13]. In recent years, researchers have been developing underwater superoleophobic surfaces (underwater oil contact angle, UOCA > 150°) in response to the oil polluting the water, as well as the adhesion of oil onto the surfaces in the oil–water–surface interface system. Here, the oil droplet on such surfaces can maintain a spherical shape and easily roll off with a small tilting angle or slight vibrations due to their unique wettability. The underwater superoleophobic surfaces have been widely used in the fields of underwater anti-fouling [14–16], crude oil transport pipelines [17,18], and oil–water separation [19,20].

Generally, most superhydrophilic surfaces exhibit underwater superoleophobicity due to the repulsive behavior of the water film to oil. For instance, Tie et al. [21] manufactured the underwater superoleophobicity surface with water contact angle (WCA) below 10° and UOCA above 150° by the simpe dipped method. Su et al. [22] fabricated a superhydrophilic/underwater superoleophobic surface by the situ free-radical polymerization method. The result shows that the the UOCA of surfaces was as large as 157.6°. Liu et al. [23] also prepared a superhydrophilic/underwater superoleophobic surface by atom transfer radical polymerization technology, and the UOCA of the surface reaches up to 150°. Chen et al. [24] presented a general strategy to fabricate underwater superoleophobic surface by tannic acid modification. In addition. many scholars prepared

the superhydrophilic/underwater superoleophobic surfaces under the guidance of bio-inspiration, for example, the structure of the fish scales. Based on the regular array of the bulges of the fish scales, numerous instructive underwater superoleophobic surfaces have been fabricated accordingly [25–28]. Yong et al. [29] manufactured the underwater superoleophobic surfaces with microgroove array structure, similar to the fish scale. The structure showed underwater oleophobicity with a UOCA greater than 155° in vertical direction, while it was only 137° in the parallel direction. Du et al. [30] fabricated a fish skin-inspired surface with a 0° WCA and 156.4° UOCA.

Generally, the durability of underwater superoleophobicity is the critical indicator for industrial applications. In the previous literature, the superhydrophilic/underwater superoleophobic surfaces are usually designed to be nanostructures to well absorb water, in which the underwater oleophobicity can be obtained. Nevertheless, the nanostructure obtained by physical or chemical methods are not robust enough [31], especially in a corrosive environment or under abrasion. Therefore, a multi-scaling structure (micro-structure and nano-structure) was proposed to fabricate a robust superhydrophilic surface by laser ablation in this paper. The nanostructure of the surface was obtained by one round of laser ablation, and the microstructure of a honeycomb pattern was formed by several rounds of laser ablation. The abrasion durability of the surface was provided by the raised honeycomb frame, and the superhydrophilic property was attributed to the nanostructure surface [32]. The prepared surface shows robust superhydrophilicity and underwater superoleophobicity, even after 6 h of corrosion and cyclic abrasion.

2. Materials and Methods

2.1. Nanosecond Laser Ablation

As shown in Figure 1, an irregular rough structure was firstly fabricated on the surface of the silicon wafer by one round of ultraviolet nanosecond laser ablation (DRACO-31S40). The ablation parameters were as follows: the central wavelength was 355 nm, the scanning time interval was 30 microseconds, the frequency was 30 kHz, the laser power was 3 W, the scanning speed was100 mm/s, the scanning displacement was 10 μm, and the spot size was 15 μm. Then, the uniform honeycomb patterns were fabricated on the rough surface by five rounds of laser ablation with the same parameters, and the ablation depth of each round was about 2 μm. To verify the robustness and hydrophilicity of the honeycomb surface, the original silicon surface, the rough surface after one round of laser ablation is prepared, as well.

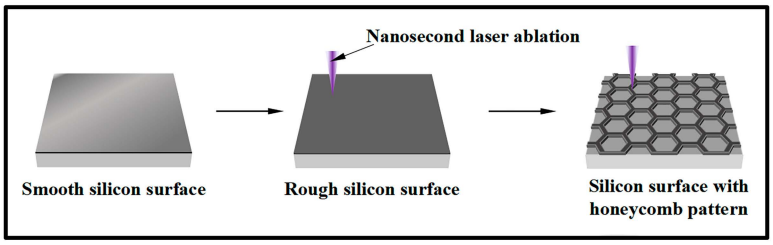


Figure 1. Sample preparation process.

2.2. Corrosion Resistance

HCl and NaOH solutions with different concentrations were used to simulate the pH values of different environments. Solutions with various pH values (pH = 1–14) were obtained by diluting standard solutions of HCl (1.0005 mol/L, Yida Technology, Quanzhou, China) and NaOH (1.0008 mol/L, Yida Technology, Guangzhou, China). Then, the samples were immersed into the solutions for 6 h (pH = 1–14), respectively. The beakers were sealed during the immersion process to reduce the solution volatilization. Then, the samples were washed with deionized water.

2.3. Abrasion Resistance

To test the mechanical durability of the prepared surface, reciprocating sliding abrasion was conducted. As shown in Figure 2, the samples were placed on 800# sandpaper with a load of 100 g weight during the test. The load applied can ensure close contact between the ablation surface and the sandpaper. Then, the sample was dragged back and forth with a displacement of 10 cm, and the speed of samples dragged on the sand paper was 10 cm/s. The abrasion cycles of 20, 40, 60, 80, 100, and 120 were tested, respectively.

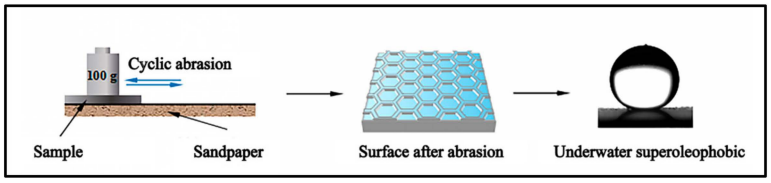


Figure 2. Friction experiment process.

2.4. Surfaces Characterization

The surface morphology of the samples was observed via a scanning electron microscope (SEM) (GeminiSEM 300, Zeiss, Jena, German), and their element content was detected by energy disperse spectroscopy (EDS) equipped on the SEM. The surfaces after corrosion were observed by an industrial USB camera (Allways, Hangzhou, China). In addition, the water contact angle the underwater oil contact angle and the rolling angle (RA) were measured by a surface tension apparatus (Dataphysics OCA20, Dataphysics, Stuttgart German).

3. Results

3.1. Surface Morphology and Elemental States

Figure 3 shows the microstructure of the silicon wafer before and after laser ablation. The original silicon surface was dark gray and smooth, as shown in Figure 3a. Then, the surface became extremely rough after one round of laser ablation (Figure 3b). Based on the rough surface, the honeycomb patterns were manufactured by continued laser ablation (Figure 3c). As can be seen in Figure 3d, the length of the honeycomb pattern is around 100 μm, and the width of the raised edge is around 20 μm. The recessed areas of the honeycomb show the nanostructures, which are beneficial to capture water droplets and, thereby, avoid oil droplets. Therefore, the microstructure of the honeycomb pattern and the nanostructure of the rough surface formed a robust superhydrophilic surface, where the abrasion durability of the surface was provided by the raised honeycomb frame, and the superhydrophilic property was attributed to the nanostructure surface. Figure 3e,f shows the results of EDS before and after laser ablation. Obviously, the content of oxygen on the rough surface increased significantly after laser ablation. It is proved that the silicon was oxidized by oxygen atoms, and the silicon oxide was formed at the top surface.

3.2. Surface Wettability

Figure 4 shows the wettability of the original silicon surface, the rough surface, and the honeycomb pattern surface. We can see that, without any treatment, the water contact angle of the original silicon surface is 50.9°. However, the contact angle decreases to 0° after one round of laser ablation, and it takes 5 s for the droplet to flatten to 0°. Furthermore, it takes only 700 ms for the water droplet to flatten to 0° for the honeycomb pattern surface. Obviously, the superhydrophilic property of the honeycomb pattern surface is better than the original silicon surface and the rough surface. Then, the underwater oil contact angle was measured in deionized water. The oil we used in this experiment is a 1,2 dichloroethane (CH_2ClCH_2Cl) reagent. As shown in Figure 4d, the UOCA is 164.9°, which means the honeycomb surface has excellent underwater superhydrophobic properties. In addition, we can see that the rolling angle is less than 1° (Figure 4e). This implies the honeycomb surface

has great anti-fouling property in water. Finally, no oil contamination was observed when the 1,2 dichloroethane droplet was forced to make contact with the honeycomb surfaces, indicating that the processed surfaces possessed an ultralow oil adhesion (Figure 4f).

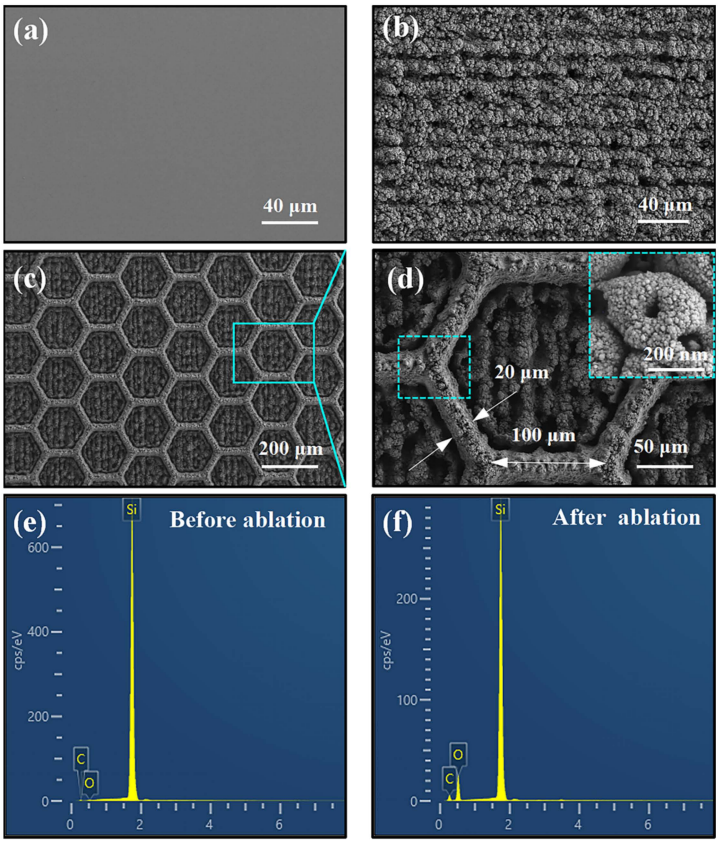


Figure 3. Surface structure and EDS detection, (**a**) the original silicon surface, (**b**) the rough surface after laser ablation, (**c**) the honeycomb pattern surface, (**d**) individual hexagonal structure on the honeycomb pattern surface, the inset is local enlargement of the raised edge, (**e**,**f**) the EDS spectra of oxygen content before and after laser ablation.

The water droplet infiltrates into the rough surface rapidly when compared to the original silicon surface. Therefore, the surface with rough structure absorbs water and forms a thin water film, and this film plays a role as an oil adhesion barrier. Moreover, although the WCA of both the rough and honeycomb pattern surface is 0°, the results showed that the water droplet flattened more rapidly on the honeycomb surface. When the water droplet contacts with the rough surface, the liquid can only flatten along the horizontal direction. However, when it contacts with the honeycomb surface, the sunken honeycomb pattern provides more space to store the water. In addition, due to the raised honeycomb frame and the sunken nanostructure, the honeycomb pattern surface has good underwater superoleophobicity.

The mechanism of wettability of the surface with rough structure can be explained by Cassie's [33] and Wenzel's models [34]. Figure 5 shows the commonly used wettability models, including Young's model [35], Wenzel's model, and Cassie's model. It is pointed out, in Cassie's model, that constructing a rough structure is an effective method to change the surface infiltration characteristics.

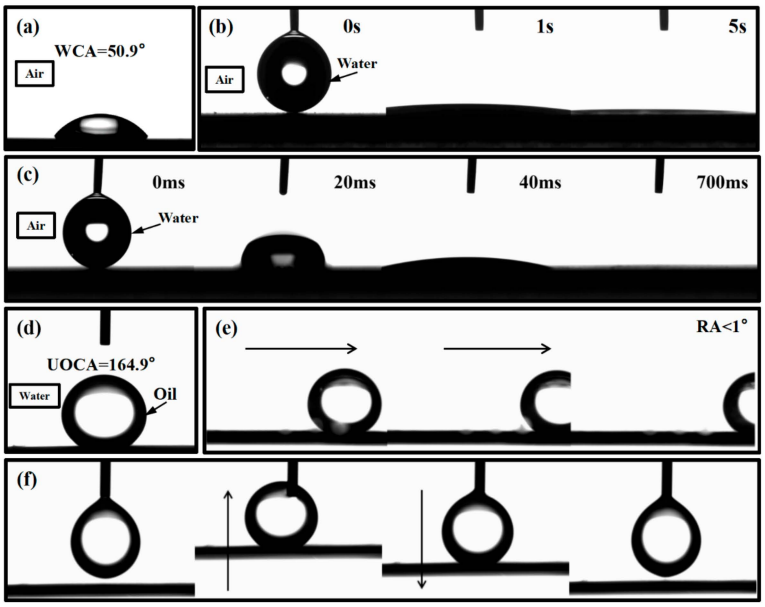


Figure 4. Surface wettability, (**a**) the water contact angle of the original silicon surface, (**b**) the expansion time of water droplet on the rough surface, (**c**) the expansion time of the water droplet on the honeycomb surface, (**d**) the underwater oil contact angle of the honeycomb surface, (**e**) the oil rolling angle of the honeycomb surface, (**f**) the oil adhesion test of the honeycomb pattern surface.

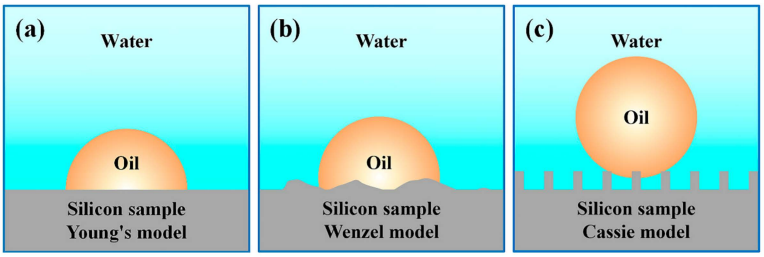


Figure 5. Underwater infiltration model, (**a**) Young's model, (**b**) the Wenzel model, and (**c**) the Cassie model.

Since water is more difficult to compress than air, as a result, the surface of the underwater Cassie model is more difficult to be infiltrated by the impact of oil droplets. So, the scale of the "water sac" on the surface can be designed to be larger, the underwater oil contact angle on the surface will be much greater, and the underwater oil rolling angle will be lesser. The underwater superoleophobic performance of the rough surface is obviously better than that of the smooth surface. It further proves the significance of the underwater Cassie model for changing the surface wettability.

In this study, two-step laser ablation was used to improve the roughness of the silicon surface. It is known that it is a disordered morphological surface after one round of laser ablation. The micro-nano structure itself has a gain effect on the hydrophilicity and oleophobicity of the silicon surface with high surface energy. Such surface properties have also been observed in other laser ablation experiments on silicon surfaces [36].

3.3. Effect of Corrosion and Abrasion on Surface Wettability

As we all know, silicon is stable and hard in relation to corrosion by acids and bases, but the silicon oxides resulting from laser ablation are susceptible to environmental influences. Figure 6 shows the structure and wettability result of the samples after the corrosion test. The experiment results show that the UOCA of the superhydrophilic/underwater superoleophobic surface with honeycomb pattern are still greater than 150° after it was immersed in the solution of pH = 1–13 for 6 h. The solution remains clear after corrosion. It means that the surface with a honeycomb pattern can maintain its superhydrophilic/underwater

superoleophobic properties after corrosion. Interestingly, it can be seen from Figure 6a that there is obvious color change and surface peeled off at the middle of the sample. This is due to the fact that partial silicon oxides of the honeycomb pattern surface were dissolved by NaOH. Local magnification of the corroded surface shows that the nanostructure is significantly reduced (Figure 6a,b). In order to further explore the effect of NaOH on the surface with honeycomb patterns, the prepared sample was immersed into the NaOH solution (pH = 14) for 6 h. The sample was taken out every 2 h and cleaned with deionized water, then re-immersed in a new NaOH solution (pH = 14). For the rough surface prepared by one round of laser ablation (Figure 6c), the oil droplets firmly adhere to the surface after being immersed in pH = 14 solution for 6 h, and it is difficult to escape from the surface, even when the oil droplet was pulled. However, the honeycomb pattern surface still maintained superoleophobicity with an UOCA of 154.5°, and the underwater oil rolling angle is less than 1° (Figure 6d–f).

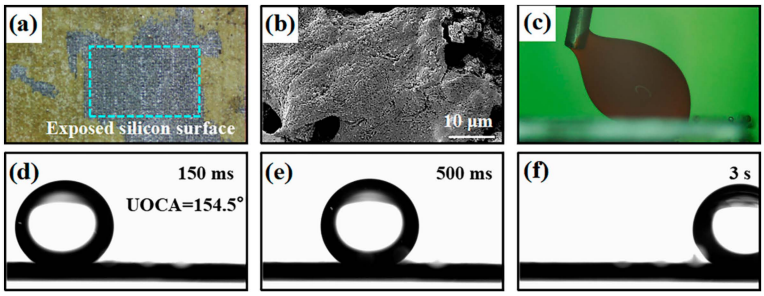


Figure 6. Surface morphology and wettability, (**a**) the surface morphology after being immersed in pH = 13 solution for 2 h, (**b**) the zoom-in picture of (**a**), (**c**) the UOCA of the rough surface after being immersed in pH = 14 solution for 6 h, (**d**–**f**) is the underwater oil rolling angle of the honeycomb pattern surface after being immersed in pH = 14 solution for 6 h.

Figure 7 shows the SEM morphologies and the EDS result of the rough surface and the honeycomb pattern surface after the corrosion. It can be seen that the rough structure formed by laser ablation on the silicon surface was completely cleaned, and the original disordered rough structure became rectangular pyramids (Figure 7a,b). Therefore, the affinity to water and high repellence to oil is lost, as shown in Figure 6c. However, even though the nanostructure of the honeycomb pattern was corroded by NaOH (pH = 14), the frame of the regular hexagon is still can be seen clearly (Figure 7e). We can see that the honeycomb pattern surface after corrosion still shows underwater superoleophobicity with a UOCA higher than 154°. The EDS result shows that the content of oxygen elements in the rough surface and the honeycomb pattern surface are greatly reduced (Figure 7c,d,g,h). The oxygen element on the rough surface reduced from 43.03% to 0.88%, and the honeycomb pattern surface reduced from 22.67% to 1.85%. This further proves that the nanostructure of the surface is corroded by the NaOH solution. The loss of the nanostructure will affect the underwater superoleophobicity. The rough surface with nanostructure loses underwater superhydrophobic properties, while the honeycomb pattern surface still maintains the microstructure of the honeycomb frame, which is consistent with the Cassie model.

Figure 8 shows the effect of abrasion on the wettability of the honeycomb pattern surface. We can see that the UOCA gradually decreases, and the WCA gradually increases with an increase in the number of abrasion cycles. The WCA increases to 7.3°, and the UOCA decreases to 151.5° after 120 cycles abrasion. Although the UOCA slightly decreases with an increase in abrasion cycles, the UOCA of the surface is still greater than 150°, which means that the underwater superoleophobic properties are still well maintained.

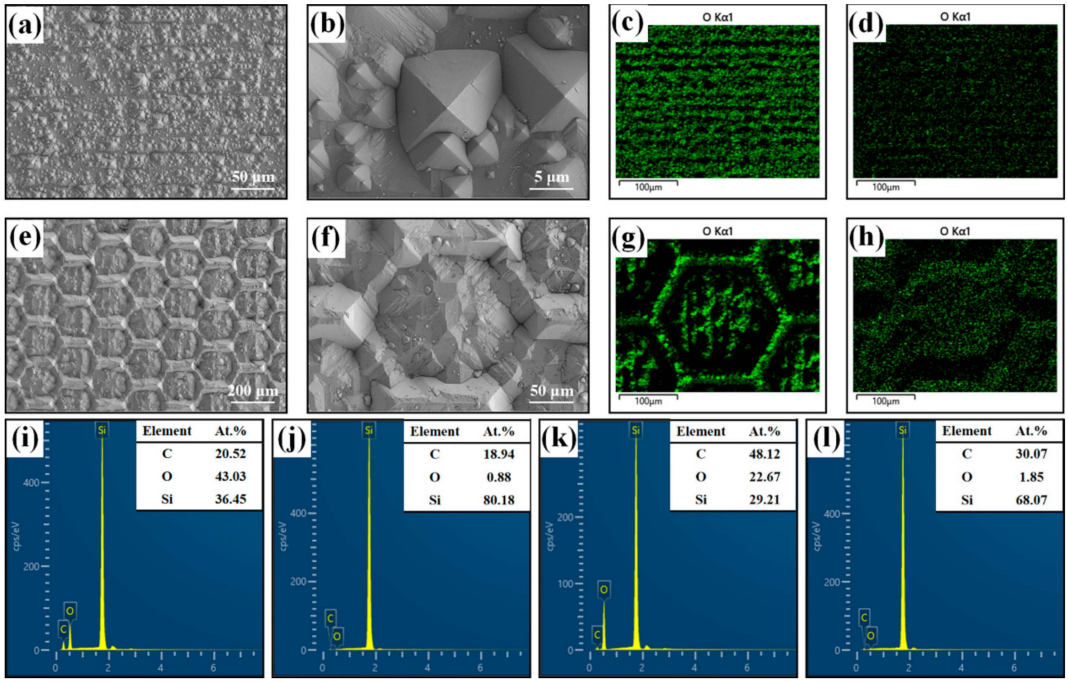


Figure 7. Surface morphology and element content, (**a**,**b**) the SEM image of the rough surface corroded by the NaOH solution (pH = 14), (**c**,**d**) the oxygen element mapping of the rough surface before and after corrosion, (**e**,**f**) the SEM image of the honeycomb pattern surface corroded by NaOH solution (pH = 14), (**g**,**h**) the oxygen element mapping of the honeycomb pattern surface before and after corrosion, (**i**–**l**) the EDS spectrum corresponding to (**c**,**d**,**g**,**h**).

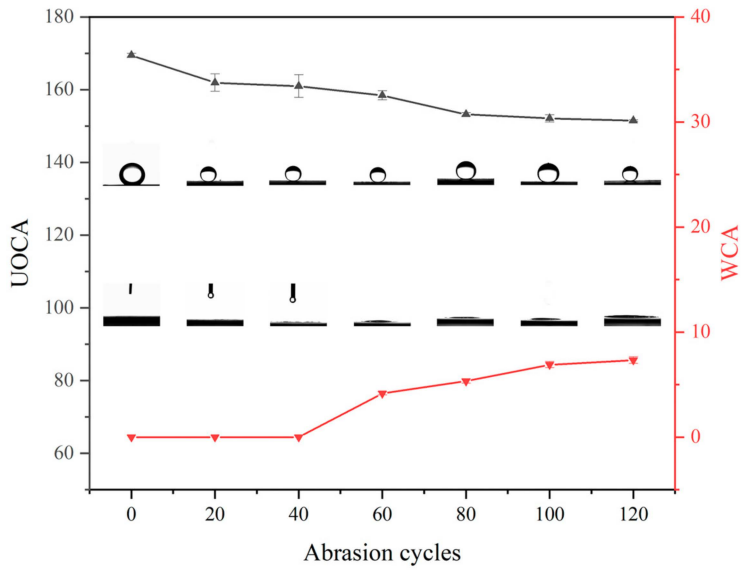


Figure 8. Effect of abrasion on water contact angle and underwater oil contact angle for honeycomb pattern surface.

Figure 9 shows the SEM images and EDS of the honeycomb pattern surface after abrasion. We can see that the microstructure of the raised honeycomb frame was abraded, while the nanostructure in the middle area of the honeycomb was undamaged. In addition, we know that the nanostructure of the surface was fabricated by laser ablation, and the silicon was oxidized in the process of ablation. Therefore, the distribution of oxygen represents the density of the nanostructure. Comparing the oxygen distribution of the honeycomb pattern surface before and after abrasion (Figure 9c,d), we can see that the

silicon oxide on the raised honeycomb frame was worn out. However, the silicon oxide inside the honeycomb was protected by the raised hexagon frame, which made it remain excellently super-hydrophilic and underwater superoleophobic.

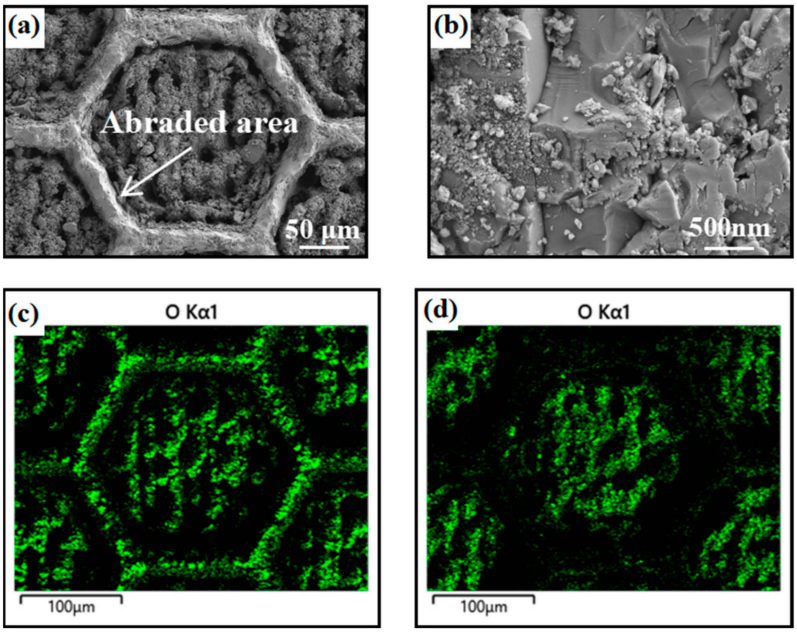


Figure 9. SEM images and EDS of the honeycomb pattern surface, (**a**,**b**) the surface morphology of the honeycomb pattern after 120 cycles abrasion, (**c**,**d**) is the oxygen distribution of the honeycomb pattern surface before and after abrasion.

4. Conclusions

In this paper, a rough surface and a multi-scaling surface combined with micro honeycomb frame structure and nanostructure was fabricated by laser ablation. The results show that the hydrophilicity and underwater superoleophobicity of the surface are greatly enhanced by the nanostructure induced by laser ablation. However, the rough surface, i.e., the nanostructure, was easily corroded by chemical solution or abraded by cyclic abrasion. Therefore, it will lose superhydrophilicity and underwater superoleophobicity. In contrast, the honeycomb pattern surface can maintain an excellent underwater superoleophobic performance after 120 cycles of abrasion or corrosion of 6 h at pH = 1–14, which is attributed to the micro-honeycomb structure, which is robust in a corrosive environment. Meanwhile, the raised honeycomb frame can protect the inside nanostructure. These findings fill the gap regarding the facile manufacturing method and robust superhydrophilic/underwater superoleophobic surface with anti-abrasion and anti-corrosion performance.

Author Contributions: D.F.: Conceptualization, Data curation, Formal analysis, Investigation, Methodology, Writing-original, Writing-review and editing. A.A.-a.: Conceptualization, Investigation, Methodology. M.C.: Conceptualization, Investigation, Methodology. J.L.: Conceptualization, Investigation, Methodology. Z.T.: Funding acquisition, Supervision, Writing-review and editing. All authors have read and agreed to the published version of the manuscript.

Funding: This research was funded by the National Science Foundation of China (52165022), the Science and Technology Project of Guizhou Province ([2020]1Y415), and the Project of Guizhou University ([2019]24).

Institutional Review Board Statement: Not applicable.

Informed Consent Statement: Not applicable.

Data Availability Statement: The data that support the findings of this study are available within the article.

Conflicts of Interest: The authors declare that they have no known competing financial interest or personal relationships that could have appeared to influence the work reported in this paper.

References

1. Sas, I.; Gorga, R.E.; Joines, J.A.; Thoney, K.A. Literature Review on Superhydrophobic Self-Cleaning Surfaces Produced by Electrospinning. *J. Polym. Sci. B Polym. Phys.* **2012**, *50*, 824. [CrossRef]
2. Zheng, S.L.; Li, C.; Zhang, Y.P.; Xiang, T.F.; Cao, Y.; Li, Q.L.; Chen, A. General Strategy towards Superhydrophobic Self-Cleaning and Anti-Corrosion Metallic Surfaces: An Example with Aluminum Alloy. *Coatings* **2021**, *11*, 788. [CrossRef]
3. Li, B.F.; Xue, S.Y.; Mu, P.; Li, J. Robust Self-Healing Graphene Oxide-Based Superhydrophobic Coatings for Efficient Corrosion Protection of Magnesium Alloys. *ACS Appl. Mater. Interfaces* **2022**, *14*, 30192. [CrossRef] [PubMed]
4. Li, B.F.; Yin, X.X.; Xue, S.Y.; Mu, P.; Li, J. Facile fabrication of graphene oxide and MOF-based superhydrophobic dual-layer coatings for enhanced corrosion protection on magnesium alloy. *Appl. Surf. Sci.* **2022**, *580*, 152305. [CrossRef]
5. Xue, S.Y.; Li, B.F.; Mu, P.; Li, J. Designing attapulgite-based self-healing superhydrophobic coatings for efficient corrosion protection of magnesium alloys. *Prog. Org. Coat.* **2022**, *170*, 106966. [CrossRef]
6. Grahama, L.A.; Agrawalb, P.; Oleschukb, R.D.; Daviesa, P.L. High-capacity ice-recrystallization endpoint assay employing superhydrophobic coatings that is equivalent to the 'splat' assay. *Cryobiology* **2018**, *18*, 138. [CrossRef]
7. Zhang, Z.; Liu, X.Y. Control of ice nucleation: Freezing and antifreeze strategies. *Chem. Soc. Rev.* **2018**, *47*, 7116. [CrossRef]
8. Liao, R.J.; Li, C.; Yuan, Y.; Duan, Y.Z.; Zhuang, A.Y. Anti-icing performance of ZnO/SiO_2/PTFE sandwich-nanostructure superhydrophobic film on glass prepared via RF magnetron sputtering. *Mater. Lett.* **2017**, *206*, 109. [CrossRef]
9. Park, S.; Jung, S.; Heo, J.; Hong, J. Facile synthesis of polysilsesquioxane toward durable superhydrophilic/superhydrophobic coatings for medical devices. *J. Ind. Eng. Chem.* **2019**, *77*, 97. [CrossRef]
10. Xun, X.W.; Zhang, Q.C.; Gan, D.Q.; Hua, J.; Luo, H.L. Low adhesion superhydrophobic AZ31B magnesium alloy surface with corrosion resistant and anti-bioadhesion properties. *Appl. Surf. Sci.* **2020**, *505*, 144566. [CrossRef]
11. Zhao, J.; Song, L.J.; Yin, J.H.; Ming, W.H. Anti-bioadhesion on hierarchically structured, superhydrophobic surfaces. *Chem. Commun.* **2013**, *49*, 9191. [CrossRef]
12. Zhao, X.; Yu, B.; Zhang, J.P. Transparent and durable superhydrophobic coatings for anti-bioadhesion. *J. Colloid Interface Sci.* **2017**, *501*, 222. [CrossRef]
13. Zhu, T.; Wu, J.R.; Zhao, N.; Cai, C.; Qian, Z.C.; Si, F.F.; Luo, H.; Guo, J.; Lai, X.; Shao, L.Q.; et al. Superhydrophobic/Superhydrophilic Janus Fabrics Reducing Blood Loss. *Adv. Healthc. Mater.* **2018**, *7*, 1701086. [CrossRef]
14. Al-Akhali, A.; Nie, K.X.; Fang, D.X.; Tang, Z.Q. Fabrication of metal-based superhydrophilic and underwater superoleophobic surfaces by laser ablation and magnetron sputtering. *Appl. Surf. Sci.* **2023**, *621*, 156829. [CrossRef]
15. Dong, Y.; Huang, C.X.; Yang, X.Y. Underwater superoleophobic and underoil superhydrophobic surface made by liquid-exfoliated MoS2 for on-demand oil-water separation. *Chem. Eng. J.* **2019**, *361*, 322. [CrossRef]
16. Liao, Z.; Wu, G.; Lee, D.; Yang, S. Ultrastable underwater anti-oil fouling coatings from spray assemblies of polyelectrolyte grafted silica nanochains. *ACS Appl. Mater. Interfaces* **2019**, *11*, 13642. [CrossRef] [PubMed]
17. Guo, Y.Z.; Li, W.P.; Zhu, L.Q.; Wang, Z.W.; Liu, H.C. Phosphoric chemical conversion coating with excellent wax-repellent Performance. *Appl. Surf. Sci.* **2012**, *259*, 356. [CrossRef]
18. Moradi, S.; Amirjahadi, S.; Danaee, I.; Soltani, B. Experimental investigation on application of industrial coatings for prevention of asphaltene deposition in the well-string. *J. Pet. Sci. Eng.* **2019**, *181*, 106095. [CrossRef]
19. Zhang, Z.; Zhang, Y.H.; Fan, H.; Wang, Y.L.; Zhou, C.; Ren, F.F.; Wu, S.Z.; Li, G.Q.; Hu, Y.L.; Li, J.W.; et al. A Janus oil barrel with tapered microhole arraysfor spontaneous high-flux spilled oil absorption and storage. *Nanoscale* **2017**, *9*, 15796. [CrossRef] [PubMed]
20. Ritchiea, A.W.; Coxa, H.J.; Barrientos-Palomo, S.N.; Sharples, G.J.; Badyal, J.P.S. Bioinspired multifunctional polymer–nanoparticle–surfactant complex nanocomposite surfaces for antibacterial oil–water separation. *Colloid Surf. A* **2019**, *560*, 352. [CrossRef]
21. Tie, L.; Li, J.; Liu, M.M.; Guo, Z.G.; Liang, Y.M.; Liu, W.M. Facile Fabrication of Superhydrophobic and Underwater Superoleophobic Coatings. *ACS Appl. Nano Mater.* **2018**, *1*, 4894. [CrossRef]
22. Su, M.J.; Liu, Y.; Li, S.H.; Fang, Z.P.; He, B.Q.; Zhang, Y.H.; Li, Y.L. A rubber-like, underwater superoleophobic hydrogel for efficient oil/water. *Sep. Chem. Eng. J.* **2019**, *361*, 364. [CrossRef]
23. Liu, S.W.; Zhou, Z.P.; Zhou, S.; Cui, J.Y.; Wang, Q.Q.; Zhang, Y.F. Fabrication of acrylamide decorated superhydrophilic and underwater superoleophobic poly(vinylidene fluoride) membranes for oil/water emulsion separation. *Taiwan Inst. Chem. E* **2019**, *95*, 300. [CrossRef]
24. Chen, Y.P.; Meng, J.X.; Zhu, Z.P.; Zhang, F.L.; Wang, L.Y.; Gu, Z.; Wang, S.T. Bio-Inspired Underwater Super Oil-Repellent Coatings for Anti-Oil Pollution. *Langmuir* **2018**, *34*, 6063. [CrossRef] [PubMed]
25. Chu, D.K.; Yin, K.; Dong, X.R.; Luo, Z.; Duan, J.A. Femtosecond laser fabrication of robust underwater superoleophobic and anti-oil surface on sapphire. *AIP Adv.* **2017**, *7*, 115224. [CrossRef]
26. Samanta, A.; Wang, H.; Shaw, S.K.; Ding, H.T. Roles of chemistry modification for laser textured metal alloys to achieve extreme surface wetting behaviors. *Mater. Des.* **2020**, *192*, 108744. [CrossRef]

27. Yong, J.L.; Chen, F.; Fang, Y.; Huo, J.L.; Yang, Q.; Zhang, J.Z.; Bian, H.; Hou, X. Bioinspired Design of Underwater Superaerophobic and Superaerophilic Surfaces by Femtosecond Laser Ablation for Anti- or Capturing Bubbles. *ACS Appl. Mater. Interfaces* **2017**, *9*, 39863. [CrossRef]
28. Qu, B.; Wang, J.; Pan, L.L.; Pan, C.; Zhou, X.H.; Gu, Z.Z. Bionic Duplication of Fresh *Navodon septentrionalis* Fish Surface Structures. *Nanomaterials* **2011**, *4*, 134860.
29. Yong, J.L.; Chen, F.; Yang, Q.; Farooq, U.; Bian, H.; Du, G.Q.; Hou, X. Controllable underwater anisotropic oil-wetting. *Appl. Phys. Lett.* **2014**, *105*, 071608. [CrossRef]
30. Du, H.Z.; Liu, F.T.; Wang, H.Y. Bio-inspired robust superhydrophilic/underwater superoleophobic coating with lubrication, anti-crude oil fouling and anti-corrosion performances. *J. Colloid Terf. Sci.* **2022**, *616*, 720. [CrossRef]
31. Tian, X.L.; Verho, T.; Ras, R.H.A. Moving superhydrophobic surfaces toward real-world applications. *Science* **2016**, *352*, 142. [CrossRef]
32. Wang, D.H.; Sun, Q.Q.; Hokkanen, M.J.; Zhang, C.L.; Lin, F.Y.; Liu, Q.; Zhu, S.P.; Zhou, T.F.; Chang, Q.; He, B.; et al. Design of robust superhydrophobic surfaces. *Nature* **2020**, *582*, 55. [CrossRef]
33. Chen, C.L.; Wang, D.; Mahmood, A.; Chen, S.; Wang, J.D. Separation Mechanism and Construction of Surfaces with Special Wettability for Oil/Water Separation. *ACS Appl. Mater. Interfaces* **2019**, *11*, 11. [CrossRef] [PubMed]
34. Ghaffari, S.; Aliofkhazraei, M.; Darband, G.B.; Zakeri, A.; Ahmadi, E. Review of superoleophobic surfaces: Evaluation, fabrication methods, and industrial applications. *Surf. Interfaces* **2019**, *17*, 100340. [CrossRef]
35. Li, F.R.; Kong, W.T.; Zhao, X.Z.; Pan, Y.L. Multifunctional TiO_2-Based Superoleophobic/Superhydrophilic Coating for Oil–Water Separation and Oil Purification. *ACS Appl. Mater. Interfaces* **2020**, *15*, 18074. [CrossRef] [PubMed]
36. Yong, J.L.; Chen, F.; Yang, Q.; Zhang, D.S.; Farooq, U.; Du, G.Q.; Hou, X. Bioinspired underwater superoleophobic surface with ultralow oil-adhesion achieved by femtosecond laser microfabrication. *J. Mater. Chem. A* **2014**, *2*, 8790. [CrossRef]

Disclaimer/Publisher's Note: The statements, opinions and data contained in all publications are solely those of the individual author(s) and contributor(s) and not of MDPI and/or the editor(s). MDPI and/or the editor(s) disclaim responsibility for any injury to people or property resulting from any ideas, methods, instructions or products referred to in the content.